Materials Transactions, Vol. 60, No. 7 (2019) pp. 1367 to 1376
Special Issue on Severe Plastic Deformation for Nanomaterials with Advanced Functionality

Critical Temperature in Bulk Ultrafine-Grained Superconductors of Nb, V, and Ta Processed by High-Pressure Torsion

Terukazu Nishizaki[1,*], Kaveh Edalati[2,3], Seungwon Lee[4], Zenji Horita[2,3], Tadahiro Akune[1], Tsutomu Nojima[5], Satoshi Iguchi[5] and Takahiko Sasaki[5]

[1]*Department of Electrical Engineering, Kyushu Sangyo University, Fukuoka 813-8503, Japan*
[2]*WPI, International Institute for Carbon-Neutral Energy Research (WPI-I2CNER), Kyushu University, Fukuoka 819-0395, Japan*
[3]*Department of Materials Science and Engineering, Faculty of Engineering, Kyushu University, Fukuoka 819-0395, Japan*
[4]*Department of Materials Design and Engineering, University of Toyama, Toyama 930-8555, Japan*
[5]*Institute for Materials Research, Tohoku University, Sendai 980-8577, Japan*

This overview describes the progressive results of the superconducting critical temperature in bulk nanostructured metals (niobium, vanadium and tantalum) processed by high-pressure torsion (HPT). Bulk nanostructured superconductors provide a new route to control superconducting property, because ultrafine-grain structures with a high density of grain boundaries, dislocations, and other crystalline defects modify the superconducting order parameter. The critical temperature T_c in Nb increases with the evolution of grain refinement owing to the quantum confinement of electrons in ultrafine grains. In V and Ta, however, T_c decreases at a certain HPT revolution number (i.e. at certain strain levels). The different behaviour of T_c in the three materials is explained by the competition effect between the quantum size effect and disorder effect; these effects are characterized by the parameters of grain size, electron mean free path, and superconducting coherence length.
[doi:10.2320/matertrans.MF201940]

(Received March 6, 2019; Accepted April 25, 2019; Published June 25, 2019)

Keywords: *high-pressure torsion, superconductivity, bulk ultrafine-grained metals, niobium, vanadium, tantalum, critical temperature, magnetization, resistivity*

1. Introduction

A superconductor is a material that shows zero electrical resistivity and perfect diamagnetism, when it is cooled below a critical temperature.[1–3] Many metallic elements, alloys, and intermetallic compounds become superconductors at low temperature. In nanostructured superconductors, superconducting properties and the vortex state are different from homogeneous bulk superconductors.[4–6] When the size of superconductors is reduced to the superconducting coherence length, the quantum-confinement of electrons and the size-dependent superconductivity has been theoretically predicted.[4–6] Recently, the nanofabrication technique has been developed and applied to superconducting metals, and the size effect of the superconducting transition has been studied on the ultrathin film of Pb[7] and the nanowire of Al.[8] Granular thin films, which consist of nanoscale grains, were also investigated;[9,10] however, the heavy disorder was introduced into superconductors during the film preparation process. In this situation, the superconductivity is in the dirty limit, so experimental results are out of the scope of theoretical studies for clean superconductors.[4–6]

The bulk nanostructured metals prepared by severe plastic deformation (SPD) are interesting candidate for studies on nanoscale superconductors. So far the SPD process for metallic materials has become an important technique in many research fields of science and engineering including physics, chemistry, material science, biology, geology, and tribology.[11–18] The SPD processes, such as high-pressure torsion (HPT), equal-channel angular pressing (ECAP), accumulative roll bonding (ARB), and multidirectional forging (MDF), effectively introduce a large plastic strain into the bulk metallic materials and thus fabricate bulk nanostructured materials that have ultrafine grains in the submicrometer or even nanometer range.[11–18] In the HPT process,[19,20] a thin disk is placed between two anvils and SPD is carried out by rotating the two anvils with respect to each other under a high pressure of several GPa.

In contrast to homogeneous bulk superconductors, bulk nanostructured superconductors generated by SPD provide a new route to control superconducting property, because ultrafine-grain structures with a high density of grain boundaries, dislocations, and other crystalline defects interact with the superconducting order parameter, which varies with the superconducting coherence length (several tens of nanometers). Recently, the HPT process has been applied to Nb,[21] Re,[22] and NbTi,[23] and enhancement of the critical temperature T_c,[21,22] upper critical field H_{c2}[21] and critical current density J_c[21] has been reported. For mechanisms of the T_c-enhancement, the increase of the superconducting order parameter due to the quantum size effect[4–6,21] and the increase of electron–electron coupling[22] have been discussed in the ultrafine-grained superconductors with a grain size comparable to the coherence length. However, the effect of SPD on the superconducting property is not simple because of competing effects on superconductivity.[24] In the SPD process, because the effect of grain refinement that enhances T_c competes with the effect of crystalline disorder that reduces T_c, it is not obvious whether T_c will rise by the SPD process. Here, disorder is a general term to express various crystal imperfections (e.g., grain boundaries, dislocations, impurities, lattice strain), which suppress the superconducting order parameter.

This overview presents the recent progress of the superconducting property in bulk ultrafine-grained metals processed by HPT. The superconducting transition is

*Corresponding author, E-mail: terukazu@ip.kyusan-u.ac.jp

examined by magnetization and resistivity measurements in HPT-processed Nb, V, and Ta (HPT-Nb, HPT-V, and HPT-Ta) as a function of the HPT revolution numbers N. It is found that the critical temperature T_c in HPT-Nb increases higher than that in high-purity single crystals in whole revolution numbers N. It is also shown that T_c in HPT-V and HPT-Ta decreases at a certain revolution number (i.e. at certain strain levels). The different behaviour of the superconductivity and the N dependence of T_c in three materials is discussed on the basis of the competition between the quantum size effect,[4–6,21] which is controlled by the grain size, and the disorder effect,[1,2,24] which depends on the process and materials. The validity of the HPT process and the direction toward improving superconducting properties are presented.

2. Experimental Procedure

2.1 Process and materials

For pure elemental superconductors, polycrystalline disks of Nb, V, and Ta with a purity of 99.9% were used as starting materials. Disks were processed by HPT at room temperature (RT) under a pressure of $P = 6$ GPa for different numbers of revolutions (Nb: $N = 0$, 1/4, 1/2, 1, 2, 5, 10, 20, V: $N = 0$, 1/8, 1/4, 1/2, 1, 2, 5, 10, 20, Ta: $N = 0$, 1/2, 2, 5, 10, 20, 50) with a rotation speed of $\omega = 1$ rpm.[25–30] Because the strain is introduced as a function of the distance R from the disk center and also the number of revolutions N, it can be characterized by the von-Mises equivalent strain as $\varepsilon = 2\pi RN/\sqrt{3}t$, where t is the thickness of the disk.

The average grain size $d = 2r_{av}$ of the starting materials of Nb, V, and Ta was estimated to be $2r_{av} = 40$–140 μm from the optical microscope images on the chemically etched surface. In the initial stage of the HPT process (i.e., $0 \leq N \leq 2$), the grain size is effectively reduced with increasing N and is a strong function of the distance R from the center as shown in Fig. 1. In the steady state (i.e., $N \geq 2$), however, the grain size hardly depends on N and R, showing an almost saturated value.[27–29] The microstructures of HPT-Nb,[27] HPT-V,[28] and HPT-Ta[29] in the steady state were observed at the position around $R \sim 3$ mm by using a Hitachi H-8100 transmission electron microscope (TEM). For HPT-Nb, the value of r_{av} was determined to be $r_{av} \sim 70$ μm ($N = 0$), 125 nm ($N = 2$) and 120 nm ($N = 5$).[27] The effect of N on the grain refinement on HPT-V and HPT-Ta is reasonably equivalent to that on HPT-Nb: $r_{av} \sim 20$ μm ($N = 0$) and 165 nm ($N = 5$) for HPT-V,[28] and $r_{av} \sim 150$ nm ($N = 5$) for HPT-Ta.[29]

For Nb, further grain refinement was achieved by low temperature-(LT-)HPT in liquid nitrogen[30] under $P = 6$ GPa for revolution numbers $N = 0$, 1/4, 1, 5, 15. The grain size of Nb was strongly reduced after LT-HPT and the estimated value of $r_{av} \sim 23$ nm for $N = 5$ was more than five times smaller than that after RT-HPT.[30]

2.2 Transport and magnetic measurements

HPT-processed disks with a diameter $\phi \sim 10$ mm and a thickness $t \sim 0.5$–0.6 mm were cut using a wire-cutting electric discharge machine and/or a low-speed precision cutter (Buehler, ISOMET-LS). To study the effect of HPT revolutions N on superconductivity, two kinds of samples were cut at a fixed position of $R = 2.5$ mm from the disk center; square plates with typical dimensions of 1×1 mm^2 and rods with square cross-sections having a ~0.5-mm width and ~9.5-mm length for magnetization and resistivity measurements, respectively (see Fig. 1 in Ref. 21)).

Electrical resistivity $\rho(T)$ was measured by a conventional dc four-probe method under a low current density of $J = 2$ A/cm^2. The noise level of the dc voltage measurements was ~0.3 nV.[31] The distance between voltage terminals was typically ~1 mm to minimize the inhomogeneity in the radial direction.[21]

Temperature T dependence of the magnetization $M(T)$ was measured using a superconducting quantum interface device (SQUID) magnetometer (Quantum Design, MPMS-XL and MPMS3).[21,23,24] For temperature dependence of the magnetization, two measurement modes were used. In the zero-field cooling (ZFC) mode, the sample is first cooled to a superconducting state (i.e., below T_c) in the zero magnetic

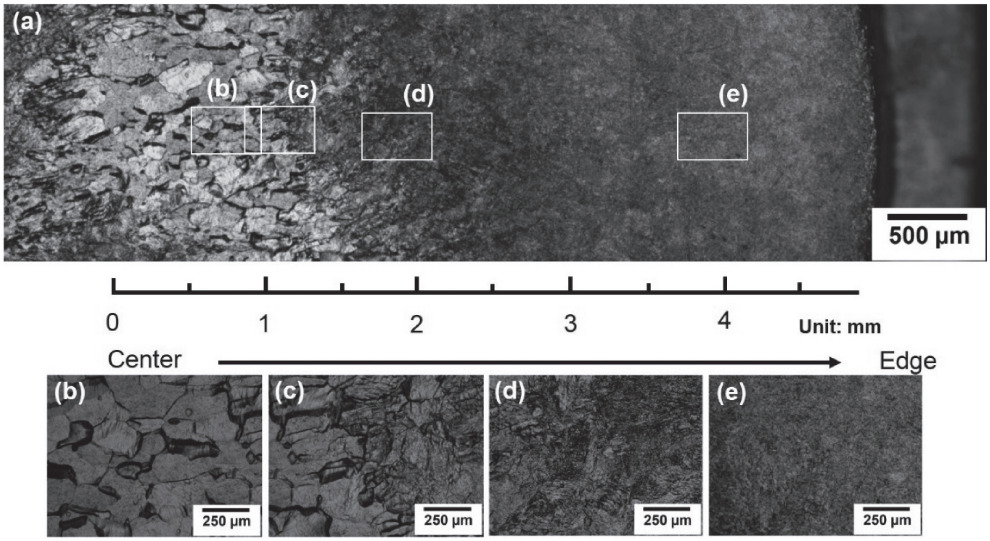

Fig. 1 Optical microscope images of HPT-Nb ($N = 1/4$). (a) Overall view from center to the edge parts. (b)–(e) Magnified views as a function of the positions shown in (a).

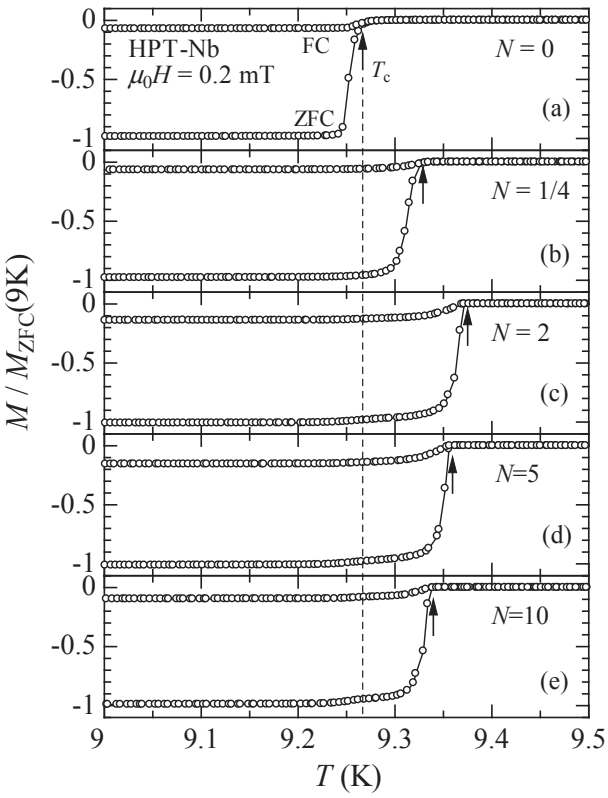

Fig. 2 Temperature dependence of the magnetization of HPT-Nb in the magnetic field $\mu_0 H = 0.2$ mT for different revolution numbers N. The magnetization $M(T)$ is normalized to -1 by a ZFC value of M(9 K). The critical temperatures are indicated by arrows.

field and then the magnetization is measured in a constant field with increasing temperature. In the field cooling (FC) mode, the magnetic field is applied in the normal state (i.e., above T_c) and the magnetization is measured with decreasing temperature.

3. Results and Discussions

3.1 Critical temperature T_c

3.1.1 HPT-Nb

Figure 2 shows the temperature dependence of the magnetization of HPT-Nb in the ZFC and FC modes before and after the HPT process at room temperature. Because the volume fraction of the superconductivity is ~100% irrespective of the HPT revolution numbers,[21] the magnetization $M(T)$ is normalized to -1 by a ZFC value of M(9 K). Critical temperatures T_c is defined by the onset of the diamagnetism as shown by arrows in Fig. 2, because perfect diamagnetism is a fundamental characteristic of superconductivity. In ideal superconductors without vortex pinning, both modes show the same diamagnetization. However, as shown in Fig. 2, the diamagnetic signal in the FC mode is very weak compared with that in the ZFC mode. The reason is that vortices are effectively trapped in the superconductor in the FC mode, as is often seen in the strong vortex-pinning superconductors.

Figure 3 shows the critical temperature T_c as a function of HPT revolution numbers N. The critical temperature before the HPT process ($N = 0$) is $T_c = 9.25$–9.26 K; the value is consistent with T_c for bulk single crystals of Nb.[32] Thus, the

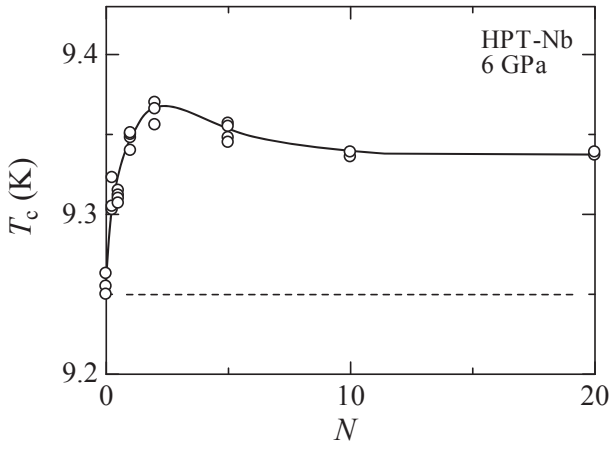

Fig. 3 Critical temperature T_c as a function of HPT revolution numbers N for HPT-Nb. Three samples were measured for each N. The broken line indicates T_c for $N = 0$ and for a single crystal of Nb.[32]

polycrystalline starting material of Nb is high quality in superconductivity, comparable to single crystals.[32] With increasing revolution numbers N, the value of T_c systematically increases and shows a maximum value ($T_c = 9.37$ K) at $N = 2$; the enhancement of T_c is $\Delta T_c/T_c \sim 1.3\%$. In the higher numbers of N (≥ 5), T_c slightly decreases and saturates to a constant value for $N = 10$–20. The value of T_c for $N = 20$ is still larger than that for $N = 0$ and for single crystals, consequently the HPT process does not reduce the superconductivity but enhances T_c in HPT-Nb. At first glance, the results are inconsistent with the general knowledge of superconductivity because, in the case of an equilibrium bulk-superconductor, the maximum value of T_c is observed in high-quality single crystals and crystalline defects reduce the superconducting order parameter in many cases.[1–3] However, ultrafine grain structures after HPT can be a trigger of the T_c-enhancement, when spatial variations of the order parameter on a scale comparable to the superconducting coherence length are positively affected by nanostructures.[4–6]

The microstructures of HPT-Nb were studied and the size of r_{av} was determined to be ~70 μm, 125 nm, and 120 nm for $N = 0$, 2, and 5, respectively. The results indicate that the grain size is effectively reduced by the HPT for $N \leq 2$ but almost saturates for $N \geq 2$. In the initial stage of HPT ($N \leq 2$), the grain size largely decreases owing to the accumulation of dislocations and the formation of subgrain boundaries with increasing revolution numbers N.[27–29,33] The subgrain boundaries are formed because of agglomeration of dislocations, and the small-angle grain boundaries transform to the large-angle grain boundaries with increasing N. In the region of higher revolution numbers ($N \geq 2$), the grain size saturates because of the balance between the generation and annihilation of dislocations. The microstructure analysis and the magnetization data indicate that T_c-enhancement is observed in the evolution process of the grain refinement.

To discuss the HPT effect on the superconducting transition, let us compare the average grain size $2r_{av}$ with the Bardeen-Cooper-Schrieffer (BCS) coherence length $\xi_0 = \hbar v_F/\pi\Delta(0)$.[1–3] Here, $\hbar$ is the reduced Planck constant, v_F the Fermi velocity, and $\Delta(0)$ the superconducting energy gap, respectively. Using the value of $\xi_0 = 39$ nm for Nb,[34,35] the

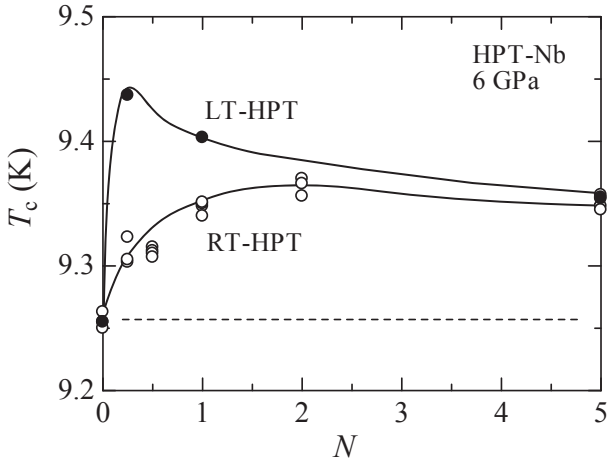

Fig. 4 Critical temperature T_c for HPT-Nb as a function of revolution numbers N for LT-HPT. The data of RT-HPT from Fig. 3 are also shown for comparison. The broken line indicates T_c for $N = 0$ and for a single crystal of Nb.[32)]

ratio of r_{av}/ξ_0 is determined to be $r_{av}/\xi_0 \sim 1800$ ($N = 0$) and $r_{av}/\xi_0 \sim 3$ ($N = 2$ and $N = 5$). Because $r_{av}/\xi_0 \sim 1800$ for $N = 0$, the large crystalline grains in HPT-Nb behaves as the three-dimensional bulk superconductivity in which no size effect is expected. However, the size r_{av} becomes comparable to ξ_0 (i.e., $r_{av}/\xi_0 \sim 3$) for $N \geq 2$. The increase of T_c can be discussed in terms of the quantum size effect that is expected in nanoscale superconductors with the confined geometry of the superconducting order parameter.[4–6)]

According to the recent theory of the nanoscale superconductors, the spatial variation of the superconducting order parameter $\Delta(r)$ and the density of states of the electrons are calculated by solving the Bogoliubov-de Genne equations[4,5)] and Gor'kov equations.[6)] Theoretical results indicate that the quantum size effect of the T_c-enhancement results from the enhancement of the superconducting order parameter, because the Cooper pair density is increased by quantum confinement in clean nanoscale superconductors.[4–6)] Because the quantum size effect is pronounced when the grain size approaches the coherence length ξ_0, the increase of T_c in HPT-Nb can be qualitatively explained by this scenario.[4–6)] However, the oscillatory behavior of T_c that is predicted in the theory[4–6)] has not been observed because of the distribution of the grain size in HPT-superconductors.

Figure 4 shows the critical temperature T_c for HPT-Nb as a function of revolution numbers N of LT-HPT. By applying the LT-HPT process in liquid nitrogen, the value of T_c remarkably increases to $T_c = 9.43$ K ($\Delta T_c/T_c \sim 1.9\%$) at $N = 1/4$. In addition, $T_c(N)$ shows the maximum value at $N_{max} \sim 1/4$ for LT-HPT; this value is much smaller than $N_{max} \sim 2$ for RT-HPT. The effective increase of T_c at low revolutions of N and the decrease of N_{max} in $T_c(N)$ indicate that LT-HPT is advantageous for preparing HPT-Nb with higher T_c. The enhancement of T_c after LT-HPT is consistent with the quantum size effect as discussed above,[4–6)] because the grain size is strongly reduced to $r_{av} \sim 23$ nm ($r_{av}/\xi_0 \sim 0.6$) for $N = 5$.

3.1.2 HPT-V

Figure 5 shows the temperature dependence of the magnetization of HPT-V in the ZFC and FC modes before and after HPT process at room temperature. The value of T_c increases only for small revolution numbers ($N = 1/8$, $1/4$, $1/2$), whereas the T_c-enhancement ($\Delta T_c/T_c \sim 0.6\%$) is smaller than that in HPT-Nb, as clearly seen in Fig. 6. With increasing revolution numbers N, T_c for $N \geq 1$ becomes smaller than that for $N = 0$ and shows a slight upturn at

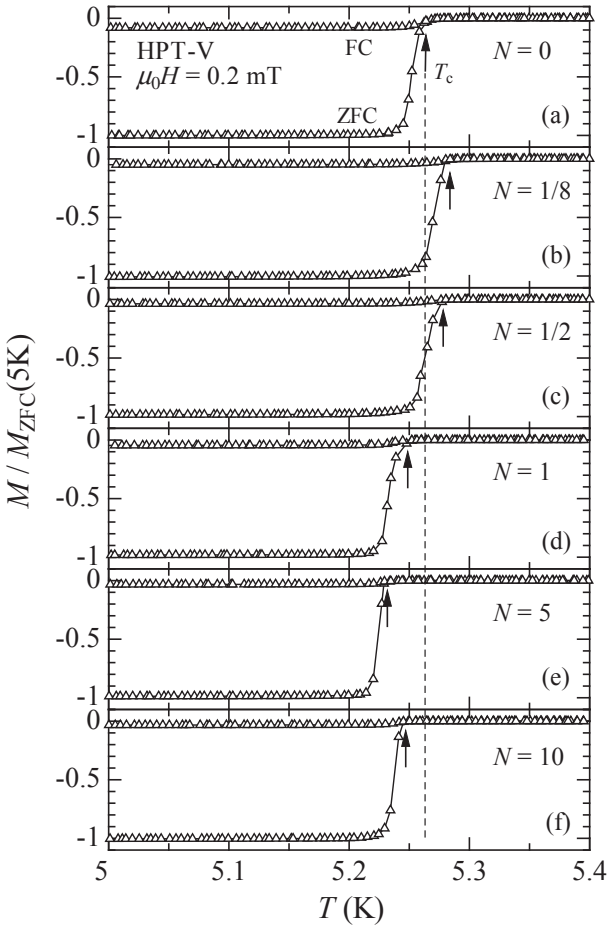

Fig. 5 Temperature dependence of the magnetization of HPT-V in the magnetic field $\mu_0 H = 0.2$ mT for different revolution numbers N. The magnetization $M(T)$ is normalized to -1 by a ZFC value of $M(5\,\mathrm{K})$. The critical temperatures are indicated by arrows.

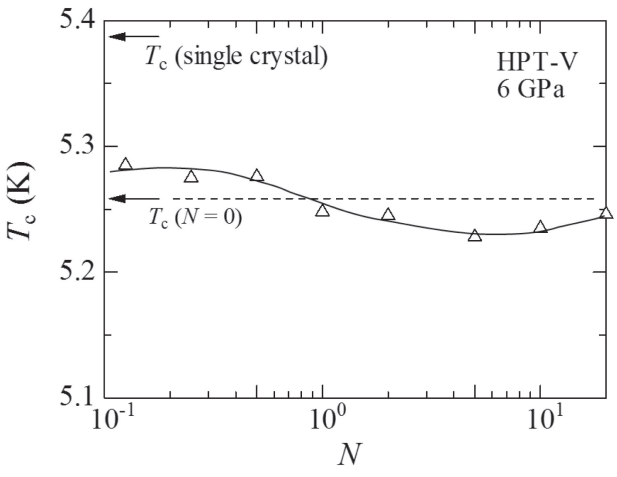

Fig. 6 Critical temperature T_c as a function of HPT revolution numbers N for HPT-V. The lower arrow with the broken line shows T_c for $N = 0$ and the upper arrow shows T_c for a single crystal of V.[38)]

$N = 20$. These results are completely different from the results in HPT-Nb. In HPT-V, the grain size $2r_{av}$ is reduced from $r_{av} \sim 20\,\mu m$ ($N = 0$) to $\sim 165\,nm$ ($N = 5$)[28] and the value is comparable to the BCS coherence length $\xi_0 = 44\,nm$[36,37] (i.e., $r_{av}/\xi_0 \sim 3.8$); this situation is similar to the condition of HPT-Nb ($N = 2$) in which the quantum size effect becomes remarkable as discussed above. The different behavior of $T_c(N)$ between HPT-V and HPT-Nb suggests the existence of competition between the quantum size effect and the disorder effect. The considerable disorder strength, which reduces T_c, is expected in the starting materials of V even if the purity is same level as Nb, because T_c ($\sim 5.26\,K$) before HPT is smaller than that for bulk single crystals of V ($T_c \sim 5.39\,K$)[38] as indicated in Fig. 6. The small amount of magnetic impurity and the inclusion of oxygen can be a candidate of the strong disorder in V.

3.1.3 HPT-Ta

Figure 7 shows the temperature dependence of the magnetization of HPT-Ta for different revolution numbers N. The critical temperature before the HPT process is $T_c \sim 4.49\,K$, which is almost same as $T_c \sim 4.483\,K$ for single crystals of Ta and highly purified Ta.[39] As shown in Fig. 7(a), the diamagnetic signal of Ta ($N = 0$) in the FC mode is stronger than that of Nb and V, indicating that the starting materials of Ta are relatively clean and the magnetic-field trapping due to crystalline defects is not so strong. Contrary to the case of HPT-Nb and HPT-V, the critical temperature T_c immediately decreases after HPT at the small revolution number of $N = 1/2$. In addition, the superconducting transition in HPT-Ta shows a characteristic two-step transition, as indicated by T_c^h and T_c^l in Fig. 7(b)–7(f). With decreasing temperature, the superconducting diamagnetic signal gradually grows below T_c^h and sharply increases below T_c^l. The volume fraction of the high-T_c phase is estimated to be ~20–30% near T_c^l, on the basis of the magnitude of the superconducting signal. Because the separation into two superconducting phases appears after HPT, the two-step transition is not due to additional impurity elements but due to the introduced nanostructure and/or the accumulated shear strain by the HPT process.

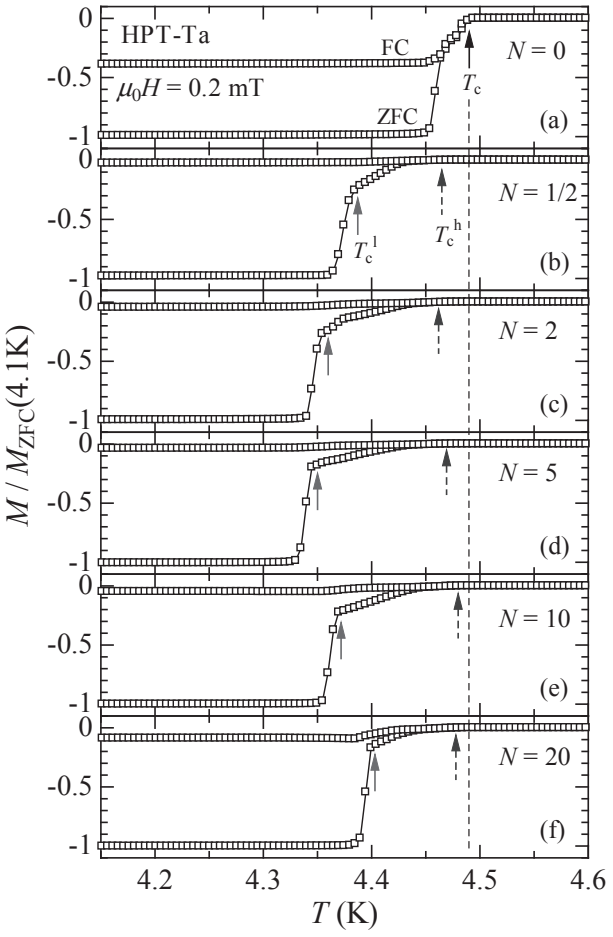

Fig. 7 Temperature dependence of the magnetization of HPT-Ta in the magnetic field $\mu_0 H = 0.2\,mT$ for different revolution numbers N. The magnetization $M(T)$ is normalized to -1 by a ZFC value of $M(4.1\,K)$. T_c^h and T_c^l indicated by arrows are critical temperatures for high-T_c and low-T_c phases of the two-step superconducting transition.

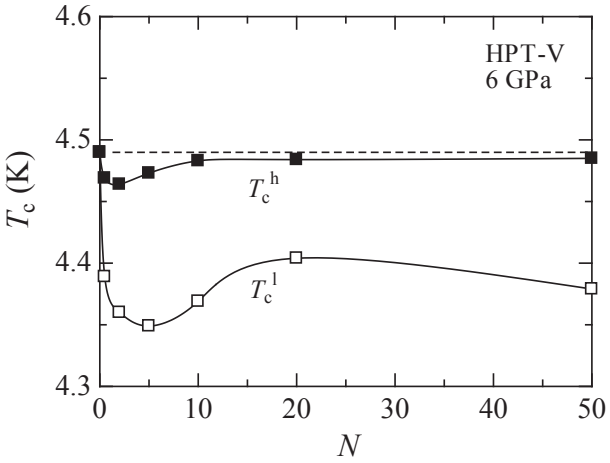

Fig. 8 Critical temperature T_c as a function of HPT revolution numbers N for HPT-Ta. T_c^h and T_c^l indicate critical temperatures for high-T_c and low-T_c phases of the two-step superconducting transition. The broken line shows T_c for $N = 0$ and for a single crystal of Ta.[39]

Figure 8 shows critical temperature T_c as a function of HPT revolution numbers N for HPT-Ta. After the HPT process, both critical temperatures (T_c^h, T_c^l) decrease in the initial stage of the HPT process (i.e., $0 < N \leq 2$). With increasing N, T_c^h increases and reaches T_c for $N = 0$ and single crystals,[39] whereas T_c^l increases and shows a broad maximum around $N \sim 20$. According to the grain-refinement process as mentioned above, the depression of $T_c^h(N)$ and $T_c^l(N)$ at low-N revolutions is closely related to the introduced nanostructures, including the crystalline defects and shear strain. After HPT, the grain size $2r_{av}$ decreases leading to $r_{av} \sim 150\,nm$ ($N = 5$)[25] and $r_{av}/\xi_0 \sim 1.7$, using $\xi_0 = 90\,nm$ for Ta.[40,41] Thus, the grain size is in the range of the quantum size effect that enhances the superconducting order parameter. However, the results suggest that the disorder effect, which reduces T_c, is considerably stronger than the quantum size effect. The increase of T_c^h and T_c^l at high revolution numbers ($N \geq 10$) can be interpreted as the recrystallization effect, which occurs in the steady state at large strains.[33]

3.2 Effect of the disorder characterized by the resistivity

3.2.1 Residual resistivity ρ_0

To discuss the degree of the disorder in HPT-Nb, HPT-V,

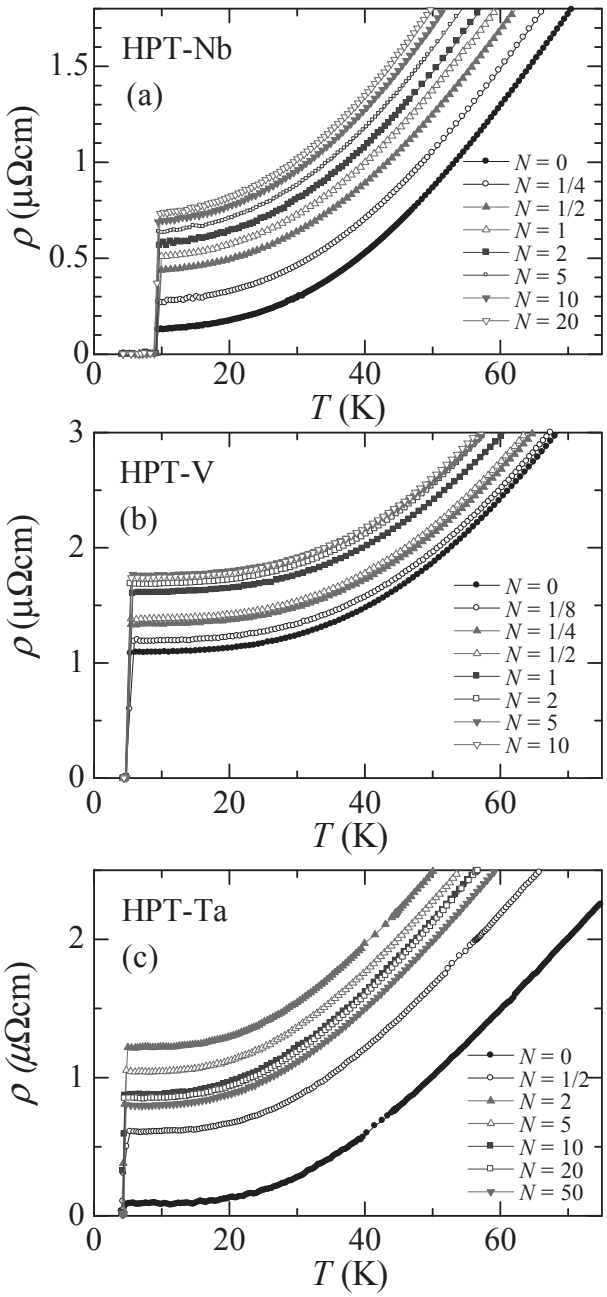

Fig. 9 Temperature dependence of the electrical resistivity $\rho(T)$ in (a) HPT-Nb, (b) HPT-V, and (c) HPT-Ta with different revolution numbers N.

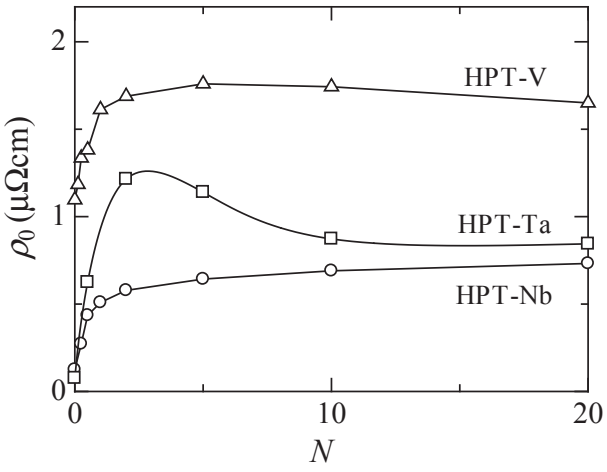

Fig. 10 Residual resistivity ρ_0 as a function of HPT revolution numbers N for HPT-Nb, HPT-V, and HPT-Ta. The value of ρ_0 is estimated from the temperature independent resistivity just above T_c.

and HPT-Ta, the temperature dependence of the electrical resistivity $\rho(T)$ has been measured. Figure 9 shows the temperature dependence of the resistivity $\rho(T)$ in (a) HPT-Nb, (b) HPT-V, and (c) HPT-V with different revolution numbers N. The resistivity is a useful parameter related to the scattering mechanism of the conduction electrons and is expressed as $\rho(T) = \rho_0 + \rho_L(T)$, according to Matthiessen's rule. Here, the temperature dependent term $\rho_L(T)$ results from the scattering by thermal phonons and the electron-electron interaction. The temperature independent term (i.e., a residual resistivity ρ_0) is originated from the scattering of electrons by static disorders that break the crystalline perfection. Therefore, the analysis of ρ_0 provides important information about the crystalline disorder and the effect of the disorder on T_c can be discussed.

Figure 10 shows ρ_0 as a function of HPT revolution numbers N for HPT-Nb, HPT-V, and HPT-Ta. The value of ρ_0 is estimated from the temperature independent resistivity just above T_c. As shown in Fig. 10, $\rho_0(N)$ in HPT-Nb steeply increases from 125 nΩcm ($N = 0$) and is saturated around ~730 nΩcm ($N = 20$) with increasing N. Although the enhancement of $\rho_0(N)$ in HPT-Nb is approximately six times after HPT ($N = 20$), $\rho_0 \sim 730$ nΩcm ($N = 20$) remains smaller than that of V before HPT ($N = 0$). In HPT-V, the value of ρ_0 is in the higher level above $\rho_0 \sim 1.1$ μΩcm ($N = 0$) and the change in $\rho_0(N)$ is smaller as compared with HPT-Nb and HPT-Ta. These results suggest that the starting materials of V already include considerable disorder, which acts as a scattering center of the conduction electrons. Dissolved gases (especially, interstitial oxygen) strongly reduce T_c in V;[42] therefore, the high-purity sample after high-temperature annealing under ultra-high vacuum[37] is a candidate as a suitable starting material for studying the intrinsic behavior of nanostructured superconductivity by HPT. In HPT-Ta, the value of ρ_0 (~76 nΩcm) for $N = 0$ is the smallest among the three materials and $\rho_0(N)$ becomes saturated near $N = 20$, with the value close to that of HPT-Nb. In the intermediate numbers of $N = 2$–5, however, $\rho_0(N)$ shows an anomalous peak structure and the peak is in good agreement with the depression of $T_c^l(N)$ and $T_c^l(N)$ in Fig. 8. This means that the decrease of $T_c^l(N)$ and $T_c^l(N)$ in HPT-Ta is caused by the enhanced electron scattering that reduces the formation of Cooper pairs.

The HPT process introduces shear strain and generated lattice defects such as dislocations and grain boundaries. In this situation, the residual resistivity ratio RRR [$\equiv \rho(300\,\mathrm{K})/\rho_0$] can be used as a measure of the purity and perfectness of the sample because it is roughly proportional to the electron mean free path l. The value of RRR strongly depends on the sample quality; for example, RRR is ~1650 in the very pure Nb crystal[43] and is ~1.5 in the heavily disordered Nb thin film.[10] Figure 11 shows critical temperature T_c as a function of RRR and inverse resistivity ratio $1/RRR$ in HPT-Nb, HPT-V, and HPT-Ta. $1/RRR$ expresses the disorder strength and increases with increasing revolution numbers N. Despite the

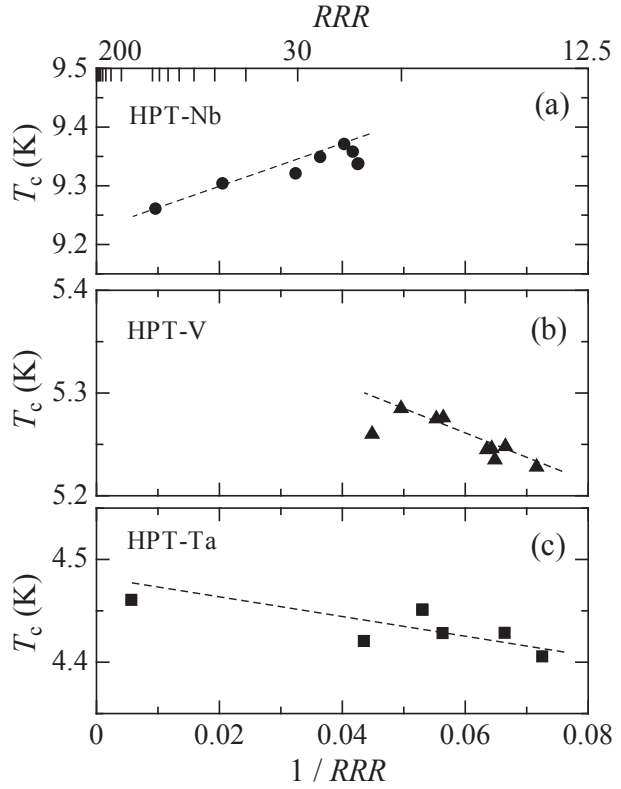

Fig. 11 Critical temperature T_c as a function of the residual resistivity ratio RRR and the inverse resistivity ratio $1/RRR$ in (a) HPT-Nb, (b) HPT-V, and (c) HPT-Ta. $1/RRR$ expresses the disorder strength. The value of T_c in HPT-Ta is obtained from the resistivity data, and the obtained T_c locates between T_c^h and T_c^l (see Fig. 8) with a similar N-dependence.

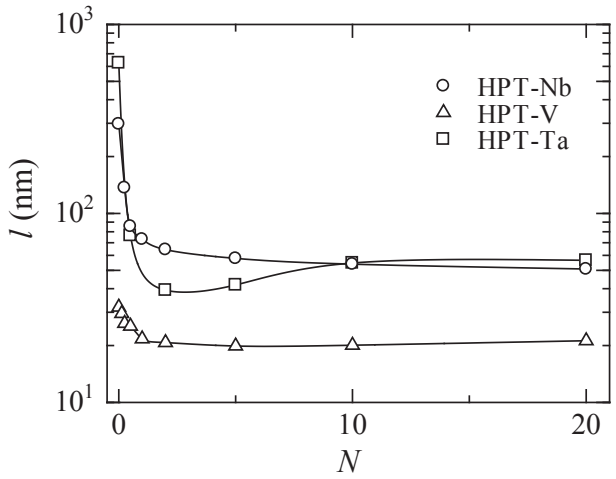

Fig. 12 Electron mean free path l as a function of HPT revolution numbers N for HPT-Nb, HPT-V, and HPT-Ta.

introduced disorder by HPT, T_c increases with increasing $1/RRR$ in HPT-Nb. As shown in Fig. 11, T_c enhancement is observed in the less disordered condition, which is experimentally determined to be $1/RRR < 0.04$ in HPT-Nb and $1/RRR < 0.049$ in HPT-V. In HPT-Nb, because grain refinement is realized in the less disordered region ($1/RRR < 0.04$), the quantum size effect[4–6] can effectively work as a T_c-enhancement mechanism.

The relation between T_c and $1/RRR$ was studied previously in thin film[44] and bulk[45,46] samples of several superconducting metals (Nb,[44] V[45] and Ta[44,46]). By controlling the impurity disorder in thin films, a monotonic decrease of T_c with $1/RRR$ was reported.[44–46] In the region with a large $1/RRR$ ($1/RRR \geq 0.04$ in HPT-Nb, ≥ 0.049 in HPT-V, and ≥ 0.053 in HPT-Ta) shown in Fig. 11, the reduction of T_c can be explained by the enhanced electron scattering at the lattice defects (i.e., the disorder effect) in the same manner in Refs. 44–46). However, the enhancement of T_c with $1/RRR$ is different from the previous results[44–46] and is a novel feature in ultrafine-grained superconductors processed by HPT.

3.2.2 Electron mean free path l and disorder strength

The effect of disorder and the scattering of the conduction electrons can be quantitatively discussed in terms of the electron mean free path $l = \pi^2 k_B^2 / e^2 v_F \gamma \rho_0$. Here, e is the electron charge, v_F is the Fermi velocity, γ is the coefficient of the electronic specific heat, and k_B is the Boltzmann constant. Figure 12 shows the electron mean free path l as a function of HPT revolution numbers N for HPT-Nb, HPT-V, and HPT-Ta, where l is calculated using the experimentally determined ρ_0 (see Fig. 10) and the values of v_F and γ described in previous papers for Nb,[47,48] V,[49] and Ta.[50,51] As shown in Fig. 12, the value of l steeply decreases in the initial stage of the HPT process (i.e., $0 < N \leq 2$), which corresponds to the accumulation of dislocations and the formation of subgrain boundaries. In the steady state with high revolution numbers, the value of l becomes almost constant.

Comparing the electron mean free path l with the grain size $2r_{av}$, let us discuss the effect of the nanostructure on electron scattering. The ratio of l to r_{av} for $N = 5$ is estimated to be $l/r_{av} \sim 0.5$ (HPT-Nb), $l/r_{av} \sim 0.12$ (HPT-V), $l/r_{av} \sim 0.28$ (HPT-Ta), using the values in Fig. 12: $l = 60$ nm (HPT-Nb), $l = 20$ nm (HPT-V), $l = 42$ nm (HPT-Ta) for $N = 5$. For HPT-Nb, the mean free path is a same level as the grain size, indicating that the mean free path roughly matches the periodicity of the grain boundaries. Because the mean free path is the average distance that the electron passes between scatterings, the grain boundaries are considered major scattering centers of electrons. In other words, electron scattering centers such as dislocations, lattice strain, and other disorders accumulate near the grain boundaries and the probability of electron scattering inside the grains is very low in HPT-Nb. On the contrary, the mean free path is much shorter than the grain size in HPT-V and HPT-Ta, so the probability of electron scattering is higher inside the grains rather than at the grain boundary. This means that the crystalline disorders introduced by HPT, which act as electron scattering centers, distribute homogeneously irrespective of the grain structures in HPT-V and HPT-Ta. According to the above analysis, the distribution of the scattering centers with respect to grain boundaries differs from material to material, and a self-cleaning effect inside grains is realized in HPT-Nb.

When discussing the effect of disorder on superconductivity, the relation between the mean free path l and the BCS coherence length ξ_0 provides an important criterion for the cleanness of the superconductivity. Superconductors with a condition $l/\xi_0 > 1$ correspond to clean superconductors and with $l/\xi_0 < 1$ correspond to dirty superconductors.[1,2,52] Figure 13 shows the critical temperature T_c as a function of

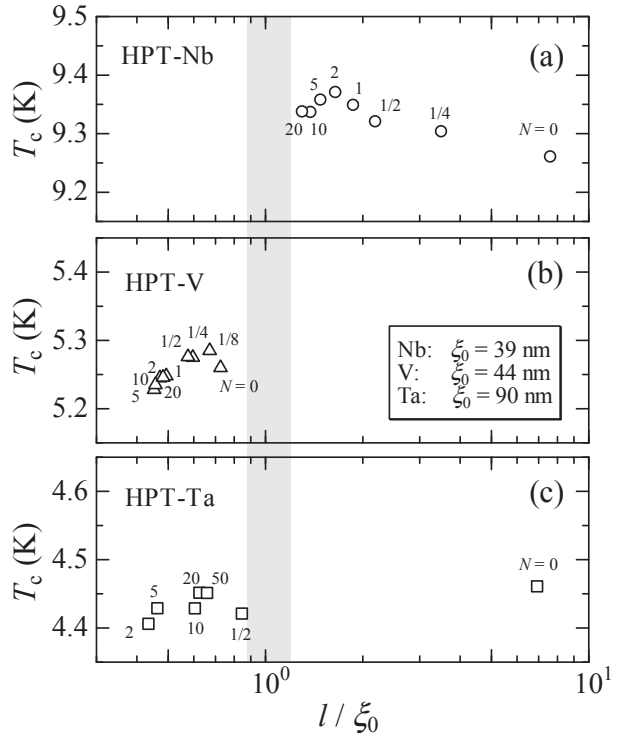

Fig. 13 Critical temperature T_c as a function of l/ξ_0 in (a) HPT-Nb, (b) HPT-V, and (c) HPT-Ta. The value of T_c in HPT-Ta is obtained from the resistivity data, and the obtained T_c locates between T_c^h and T_c^l (see Fig. 8) with a similar N-dependence. The shaded region expresses the border between clean and dirty superconductivity (i.e., $l/\xi_0 \sim 1$). The revolution numbers are given near the data points.

l/ξ_0 in (a) HPT-Nb, (b) HPT-V, and (c) HPT-Ta. The starting materials ($N = 0$) of both Nb and Ta are in the clean limit before HPT. In HPT-Nb, the parameter of l/ξ_0 decreases with increasing N, but the superconducting transition for $N = 20$ still occurs in the clean region. This is a reason that the effect of the disorder is not strong and the quantum size effect that enhances T_c is remarkable in HPT-Nb.

In HPT-V, differently form the case of HPT-Nb and HPT-Ta, the starting material of HPT-V ($N = 0$) shows dirty superconductivity. However, a small enhancement of T_c is observed for revolution numbers $N \leq 1/2$. The result may be related to HPT-V ($N = 0$) being not in the dirty limit ($l/\xi_0 \ll 1$) with strong disorder but close to the moderate level of disorder ($l/\xi_0 \sim 1$), as shown in Fig. 13(b). According to this discussion, T_c in HPT-V is expected to increase more if ultrafine-grained structures are introduced in the clean starting material of V with clean superconductivity ($l/\xi_0 > 1$).

In HPT-Ta, on the contrary, the transformation from a clean to dirty superconductor occurs immediately after the HPT process for $N \geq 1/2$. The drastic change in l/ξ_0 is caused by the increase of scattering centers inside the grains and the relatively large BCS coherence length ξ_0. According to the recent theory of nanoscale superconductors in the presence of the impurity disorder,[53] the disorder effect on T_c in the nanoscale superconductor is stronger than that expected by Anderson's theorem.[52] The theory[53] states that the suppression of T_c in the ultrafine-grained superconductor is larger than that in the coarse grained or homogeneous bulk superconductor. Therefore, the drastic decrease of T_c in the initial stage of the HPT process is consistent with the theory,[53] which indicates the enhancement of the disorder effect.

According to the above results, the different behavior of $T_c(N)$ among HPT-Nb, HPT-V, and HPT-V can be explained by the competition between two opposite effects: the quantum size effect[4–6] (Fig. 14(a)) and the disorder effect[52] (Fig. 14(b)). The quantum size effect is remarkable and the value of T_c increases when the grain size approaches ξ_0 as shown in Fig. 14(a); this situation is realized with increasing N in the initial stage of the HPT process ($0 < N \leq 2$).

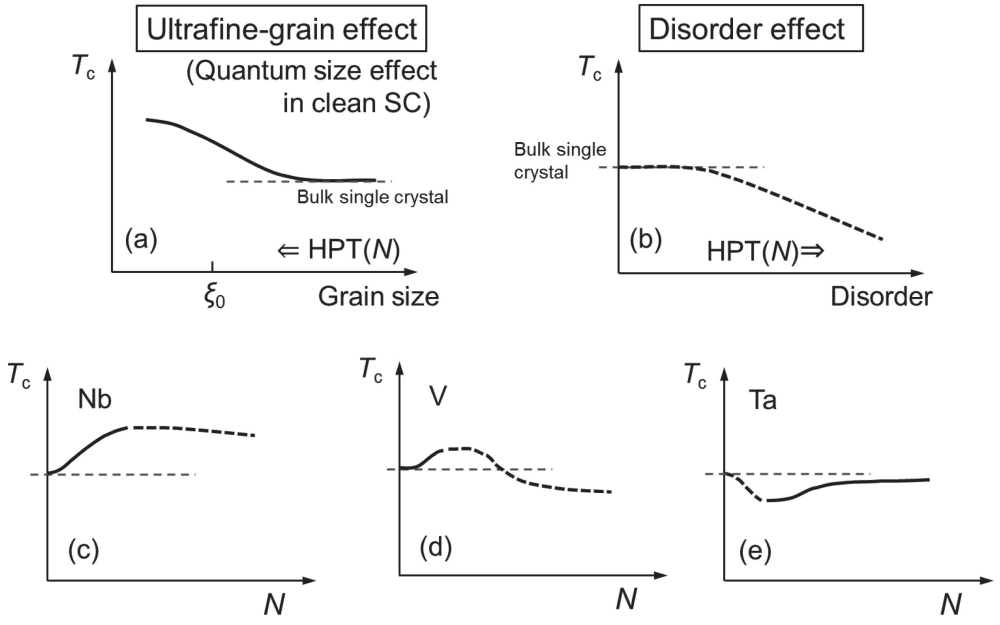

Fig. 14 Schematic drawings of (a) the quantum size effect on critical temperature T_c and (b) the disorder effect on T_c for HPT-processed superconductors. The different N-dependence of T_c in (c) HPT-Nb, (d) HPT-V, and (e) HPT-Ta is schematically explained by the competition between the two different effects.

Because the crystalline disorder masks the quantum size effect, the T_c-enhancement is most striking in clean limit superconductors.[4–6] As shown in Fig. 14(b), disorder is introduced by HPT and T_c decreases with revolution numbers N. The degree of the disorder depends on both the density and the spatial distribution of the scattering centers such as grain boundaries, dislocations and lattice strain.

The different N-dependence of T_c in HPT-Nb, HPT-V, and HPT-Ta is schematically illustrated in Fig. 14(c), 14(d), and 14(e). In HPT-Nb, the grain size is reduced under the condition of the clean superconductor (i.e., $l/\xi_0 > 1$) after the HPT process. Thus, the quantum size effect, which enhances T_c, is more of a major effect than the disorder effect (see Fig. 14(c)). Therefore, T_c-enhancement is observed in the all revolution numbers processed ($0 < N \leq 20$). In HPT-V, the disorder effect is stronger than the quantum size effect (see Fig. 14(d)) because the starting material of V already includes considerable disorder and the superconductivity is in the dirty region ($l/\xi_0 < 1$). Therefore, T_c slightly increases for the narrow revolution numbers ($1/8 \leq N \leq 1/2$) and decreases for the wide numbers ($1 \leq N \leq 20$). In HPT-Ta, clean superconductivity ($l/\xi_0 > 1$) transforms into dirty superconductivity ($l/\xi_0 < 1$) immediately after the HPT process ($N \geq 1/2$). The result indicates that the disorder effect is stronger than the quantum size effect in the initial stage of the HPT process (see Fig. 14(e)). Therefore, T_c steeply decreases for the small revolution numbers ($0 \leq N \leq 2$). For HPT-V and HPT-Ta, T_c at high revolution numbers ($N \geq 10$) increases toward the initial value for $N = 0$ (see Figs. 6 and 8), suggesting the recrystallization effect due to the disappearance of dislocations.[33] The different N-dependence of T_c between HPT-Nb and HPT-Ta in the initial stage of HPT can be explained by whether electron scattering centers exist inside the grains according to the parameter of l/r_{av} mentioned above. T_c increases when the scattering centers are hardly within the grains (HPT-Nb: Figs. 3 and 14(c)) but decreases when the scattering centers increase inside the grains with the condition of $l < r_{av}$ (HPT-Ta: Figs. 8 and 14(e)).

4. Conclusion

Magnetization and resistivity measurements were performed on HPT-processed Nb, V, and Ta, to study the effect of SPD on superconducting properties in ultrafine-grained metals. The following conclusions were obtained:

(1) HPT-Nb: The critical temperature T_c increases with the evolution process of grain refinement. The grain size is reduced under the condition of the clean superconductor (i.e., $l/\xi_0 > 1$). Thus, the quantum size effect, which enhances T_c, is more significant than the disorder effect.
(2) HPT-V: The T_c increment is observed only in the small N region ($N = 1/8, 1/4, 1/2$), but T_c turns to decrease with increasing N. The small T_c enhancement in the initial stage and T_c reduction in the wide range of N indicate that the disorder effect is stronger than the quantum size effect, because the superconductivity is in the dirty region ($l/\xi_0 < 1$).
(3) HPT-Ta: T_c steeply decreases in the initial stage of the HPT process ($0 \leq N \leq 2$). The result is explained by the transformation from clean superconductivity ($l/\xi_0 > 1$) for $N = 0$ to dirty superconductivity ($l/\xi_0 < 1$) for $N \geq 1/2$.
(4) The different behavior of $T_c(N)$ in HPT-Nb, HPT-V, and HPT-Ta is successfully explained by the quantum size effect, which enhances T_c, competing with the disorder effect, which reduces T_c. The quantum size effect is characterized by the parameter r_{av}/ξ_0, and the disorder strength is characterized by the parameters l/r_{av} and l/ξ_0.
(5) T_c in HPT-V is expected to increase more if ultra-fine grain structures are introduced in the clean starting material of V with the relation of $l/\xi_0 > 1$.
(6) The HPT process has a great advantage for producing bulk nanostructured superconductors with higher T_c. The ultrafine-grained structure with a grain size comparable to ξ_0 and clean superconductivity inside the grains provide a novel route of T_c enhancement.

Acknowledgments

The authors are grateful to Professors M. Kato and T. Ishida of Osaka Prefecture University and Professor M. Mito of Kyushu Institute of Technology for fruitful discussions. The author (T.N.) is also grateful to Mr. S. Terada and Mr. Y. Matsuzaki of Kyushu Sangyo University for their assistance with resistivity measurements. This work was supported by JSPS KAKENHI (Grant Number 16K05460). The magnetization measurements were partly performed at the Advanced Instruments Center at Kyushu Sangyo University. The HPT process was carried out in the International Research Center on Giant Straining for Advanced Materials (IRC-GSAM) at Kyushu University.

REFERENCES

1) P.G. de Gennes: *Superconductivity of Metals and Alloys*, (Perseus Books Publishing, L.L.C., USA, 1999).
2) M. Tinkham: *Introduction to Superconductivity*, (McGraw-Hill, Inc., Singapore, 1996).
3) C.P. Poole, Jr., H.A. Farach and R.J. Creswick: *Superconductivity*, (Academic Press, USA, 1995).
4) M.D. Croitoru, A.A. Shanenko and F.M. Peeters: Phys. Rev. B **76** (2007) 024511.
5) H. Suematsu, M. Kato and T. Ishida: J. Phys.: Conf. Ser. **150** (2009) 052250.
6) M. Umeda, M. Kato and O. Sato: IEEE Trans. Appl. Supercond. **26** (2016) 8600104.
7) Y. Guo, Y.-F. Zhang, X.-Y. Bao, T.-Z. Han, Z. Tang, L.-X. Zhang, W.-G. Zhu, E.G. Wang, Q. Niu, Z.Q. Qiu, J.-F. Jia, Z.-X. Zhao and Q.-K. Xue: Science **306** (2004) 1915–1917.
8) M. Savolainen, V. Touboltsev, P. Koppinen, K.-P. Riikonen and K. Arutyunov: Appl. Phys. A **79** (2004) 1769–1773.
9) B. Abeles, R.W. Cohen and G.W. Cullen: Phys. Rev. Lett. **17** (1966) 632–634.
10) S. Bose, P. Raychaudhuri, R. Banerjee and P. Ayyub: Phys. Rev. B **74** (2006) 224502.
11) M.J. Zehetbauer and Y.T. Zhu: *Bulk Nanostructured Materials*, (Wiley-VCH, Weinheim, 2009).
12) B.S. Altan: *Severe Plastic Deformation*, (Nova Science Publishers, New York, 2006).
13) R.Z. Valiev, A.P. Zhilyaev and T.G. Langdon: *Bulk Nanostructured Materials: Fundamentals and Applications*, (John Wiley & Sons, New Jersey, 2014).
14) I. Sabirov, N.A. Enikeev, M.Yu. Murashkin and R.Z. Valiev: *Bulk*

Nanostructured Materials with Multifunctional Properties, (Springer, New York, 2015).
15) R.Z. Valiev, Y. Estrin, Z. Horita, T.G. Langdon, M.J. Zehetbauer and Y. Zhu: JOM **58** (2006) 33–39.
16) K. Edalati: Proceedings of the International Workshop on Giant Straining for Advanced Materials (GSAM2015), ed. by K. Edalati, Y. Ikoma and Z. Horita, (IRC-GSAM, Kyushu University, 2016) pp.1–3.
17) R.Z. Valiev, O.A. Kaibyshev, R.I. Kuznetsov, R.S. Musalimov and N.K. Tsenev: Dokl. Akad. Nauk SSSR **301** (1988) 864–866.
18) R.Z. Valiev, R.R. Mulyukov and V.V. Ovchinnikov: Philos. Mag. Lett. **62** (1990) 253–256.
19) P.W. Bridgman: Phys. Rev. **48** (1935) 825–847.
20) A.P. Zhilyaev and T.G. Langdon: Prog. Mater. Sci. **53** (2008) 893–979.
21) T. Nishizaki, S. Lee, Z. Horita, T. Sasaki and N. Kobayashi: Physica C **493** (2013) 132–135.
22) M. Mito, H. Matsui, K. Tsuruta, T. Yamaguchi, K. Nakamura, H. Deguchi, N. Shirakawa, H. Adachi, T. Yamasaki, H. Iwaoka, Y. Ikoma and Z. Horita: Sci. Rep. **6** (2016) 36337.
23) K. Edalati, T. Daio, S. Lee, Z. Horita, T. Nishizaki, T. Akune, T. Nojima and T. Sasaki: Acta Mater. **80** (2014) 149–158.
24) T. Nishizaki: Proceedings of the International Workshop on Giant Straining for Advanced Materials (GSAM2016), ed. by K. Edalati, Y. Ikoma and Z. Horita, (IRC-GSAM, Kyushu University, 2016) pp. 47–50.
25) K. Edalati and Z. Horita: Acta Mater. **59** (2011) 6831–6836.
26) K. Edalati and Z. Horita: Scr. Mater. **64** (2011) 161–164.
27) S. Lee and Z. Horita: Mater. Trans. **53** (2012) 38–45.
28) S. Lee, K. Edalati and Z. Horita: Mater. Trans. **51** (2010) 1072–1079.
29) S. Lee and Z. Horita: private communication.
30) K. Edalati, J.M. Cubero-Sesin, A. Alhamidi, I. Mohamed and Z. Horita: Mater. Sci. Eng. A **613** (2014) 103–110.
31) T. Nishizaki, T. Naito, S. Okayasu, A. Iwase and N. Nobayashi: Phys. Rev. B **61** (2000) 3649–3654.
32) D.K. Finnemore, T.F. Stromberg and C.A. Swenson: Phys. Rev. **149** (1966) 231–243.
33) K. Edalati, T. Fujioka and Z. Horita: Mater. Sci. Eng. A **497** (2008) 168–173.
34) J.E. Ostenson and D.K. Finnemore: Phys. Rev. Lett. **22** (1969) 188–190.
35) J. Kirschenbaum: Phys. Rev. B **12** (1975) 3690–3696.
36) R. Rademaugh and P.H. Keesom: Phys. Rev. **149** (1966) 217–231.
37) S.T. Sekula and R.H. Kernohan: Phys. Rev. B **5** (1972) 904–911.
38) S.J. Williamson: Phys. Rev. B **2** (1970) 3545–3556.
39) J.L. Budnick: Phys. Rev. **119** (1960) 1578–1586.
40) J.J. Hauser and H.C. Theuerer: Phys. Rev. **134** (1964) A198–A205.
41) J. Auer and H. Ullmaier: Phys. Rev. B **7** (1973) 136–145.
42) W. DeSorbo: Phys. Rev. **132** (1963) 107–121.
43) G.W. Webb: Phys. Rev. **181** (1969) 1127–1135.
44) D. Gerstenberg and P.M. Hall: J. Electrochem. Soc. **111** (1964) 936–942.
45) R. Radebaugh and P.H. Keesom: Phys. Rev. **149** (1966) 209–215.
46) J.I. Budnick: Phys. Rev. **119** (1960) 1578–1586.
47) A.F. Mayadas, R.B. Laibowitz and J.J. Cuomo: J. Appl. Phys. **43** (1972) 1287–1289.
48) S.H. Autler and E.S. Rosenbulm: Phys. Rev. Lett. **9** (1962) 489–493.
49) R. Radebaugh and P.H. Keesom: Phys. Rev. **149** (1966) 209–216.
50) L.Y. Shen: Phys. Rev. Lett. **24** (1970) 1104–1107.
51) D. White, C. Chou and H.L. Johnston: Phys. Rev. **109** (1958) 797–802.
52) P.W. Anderson: J. Phys. Chem. Solids **11** (1959) 26–30.
53) M. Umeda and M. Kato: J. Phys. Soc. Jpn. (2019) submitted.